



**European volcanological supersite in Iceland:
a monitoring system and network for the future**

Report

Radiative transfer model and ash loading from satellites

| | | |
|------------------------------|---|--|
| Work Package: | <i>Distribution and description of eruptive products</i> | |
| Work Package number: | 8 | |
| Deliverable: | <i>Radiative transfer model and ash loading from satellites</i> | |
| Deliverable number: | 8.1. | |
| Type of Activity | <i>RTD</i> | |
| Responsible activity leader: | <i>Frank S. Marzano, CETEMPS</i> | |
| Responsible participant: | <i>CETEMPS, NILU</i> | |
| Authors: | <i>Mario Montopoli, CETEMPS Domenico Cimini, CETEMPS Arve Kylling, NILU Frank S. Marzano, CETEMPS</i> | |
| Type of Deliverable: | <i>Report</i> [X] | <i>Demonstrator</i> [] |
| | <i>Prototype</i> [] | <i>Other</i> [] |
| Dissemination level: | <i>Public</i> [X] | <i>Restricted Designated Group</i> [] |
| | <i>Prog. Participants</i> [] | <i>Confidential (consortium)</i> [] |



**Seventh Framework Programme
EC project number: 308377**

Abstract.

The potential of satellite passive microwaves sensors to provide quantitative information about near-source volcanic ash cloud parameters during an eruptive event is analyzed from both numerical and experimental point of view. To this aim ground-based microwave (MW) weather radar observations and spaceborne MW radiometer forward model simulations are used. The latter are based on the volcanic plume numerical two-dimensional simulations (named ATHAM), coupled with a radiative transfer model, based on the Eddington scheme and Mie scattering approximation (named SDSU). The study area is the Icelandic subglacial volcanic region and the analyzed case study is that of the Grímsvötn eruption on May 2011. The tuning of ATHAM parameterizations has been carried out using available ground data of the Grímsvötn volcanic eruptions. Sensitivity tests, based on the variation of some environmental conditions like the terrain emissivity, water vapor and ice concentration within the volcanic plume, are also accomplished in order to investigate the behavior of the observed space-based brightness temperatures and their variance.

The reverse absorption technique is often used to detect volcanic ash clouds from thermal infrared satellite measurements. From these measurements effective particle radius and mass loading may be estimated using radiative transfer modelling. The radiative transfer modelling usually assumes that the ash particles are spherical. Thermal infrared optical properties of highly irregular and porous ash particles were calculated and compared with mass- and volume-equivalent spherical models. Furthermore, brightness temperatures pertinent to satellite observing geometry were calculated for the different ash particle shapes. Non-spherical shapes and volume-equivalent spheres were found to produce a detectable ash signal for larger particle sizes than mass-equivalent spheres. The assumption of mass-equivalent spheres for ash mass loading estimates was found to underestimate mass loading compared to morphologically complex inhomogeneous ash particles. The underestimate increases with the mass loading. For an ash cloud recorded during the Eyjafjallajökull 2010 eruption, the mass-equivalent spheres underestimate the total mass of the ash cloud by approximately 30% compared to the morphologically complex inhomogeneous particles

Contents

- 1. INTRODUCTION TO MICROWAVE RADIATIVE TRANSFER MODEL..... 3
- 2. MICROWAVE AND NUMERICAL VOLCANIC PLUME MODEL..... 3
 - 2.1 Volcanic plume model3
 - 2.1 Microwave sensor response simulator6
- 3. NUMERICAL RESULTS OF MICROWAVE SIMULATOR 7
 - 3.1 Microwave brightness temperature simulations8
 - 3.2 Ash loading estimate and surface emission sensitivity9
 - 3.3 Considerations..... 10
- 4. IMPROVED INFRARED RETRIEVAL OF ASH MASS LOADING 11
- 5. ASH PARTICLE OPTICAL PROPERTIES 12
 - 5.1 Particle shapes 12
 - 5.2 Single scattering optical properties 12
- 6. INFRARED RADIATIVE TRANSFER SIMULATION SETUP AND RESULTS 13
 - 6.1 Numerical results 13
 - 6.2 Discussion 14
- REFERENCES..... 16

1. INTRODUCTION TO MICROWAVE RADIATIVE TRANSFER MODEL

Traditionally, the monitoring of ash plumes is performed exploiting thermal infrared and optical channels of spaceborne radiometers (Wen and Rose, 1994; Gangale et al., 2010). These measurements can be obtained from sensors aboard geosynchronous-earth-orbit (GEO) and low-earth-orbit (LEO) satellites, thus offering different spatial and temporal resolutions for ash cloud remote sensing. For GEO platforms the advantage of a rapid sampling rate of the earth scene has the disadvantage of a lower spatial resolution (typically larger than few kilometers). For LEO the revisit time may be even longer than 12 hours but with spatial resolutions that vary from several kilometers down to meters depending on the wavelength used by the sensor aboard on LEO platforms. Moreover, thermal infrared and optical channels may suffer from strong ash cloud opacity (very often mixed with water cloud) due to the significant radiation extinction especially in the proximity of the volcanic source. In this respect, the exploitation of the microwave passive sensors may represent a good opportunity to observe the ash cloud, despite some inherent limitations (Delene et al., 1996; Grody and Basist, 1996). The aim of this work is to investigate the potential use of spaceborne microwave passive sensors for estimating volcanic plume parameters by comparing them to and combining them with results from a numerical model.

Numerical simulations of volcanic eruption plumes are generated using the Active Tracer High-Resolution Atmospheric Model (ATHAM) (Textor et al., 2006; Oberhuber et al., 1998; Textor et al., 2003). ATHAM outputs together with the Satellite Data Simulator Unit (SDSU) (Masunaga et al., 2010) are used to generate synthetic observations of satellite-based microwave brightness temperature. SDSU is a radiative transfer model, which includes both multiple scattering and Mie extinction modules for ensembles of spherical particles. SDSU is able to simulate the response of active and passive remote sensors from microwaves to visible wavelengths. While ATHAM is a plume model specifically designed for volcanic studies, SDSU has been modified (as described in this study) to accurately describe the ash cloud electromagnetic and microphysical features as well as to ingest the outputs of ATHAM. Both ATHAM and SDSU simulations are performed in a two-dimensional (2D) framework.

The role of the ATHAM 2D model in this study is to provide a likely realization of a volcanic eruption plume without claiming to exactly reproduce the case study of the Grímsvötn eruption that we analyze in this work. The actual observations which will be considered in the next activity refer to the case study of the Grímsvötn volcanic eruption, which occurred on May 2011 in Iceland. Measurements include data from the Special Sensor Microwave Imager/Sounder (SSMIS) on a LEO platform during the Grímsvötn eruption on May 22nd and a C-band ground based weather radar, which observed the same event from a distance of approximately 260 km.

2. MICROWAVE AND NUMERICAL VOLCANIC PLUME MODEL

In order to analyze and interpret the microwave radiometric signatures from space, a coupled microwave and volcanic plume model is set up. The adjustment of model parameters exploits information that we collected from the current and past sub-glacial Icelandic eruptions. The next two sections describe the physical and electromagnetic model components.

2.1 Volcanic plume model

ATHAM is a non-hydrostatic numerical model with applications across a broad range of atmospheric problems. In the volcanic configuration it has been used to study the effect of large volcanic eruptions on stratospheric chemistry and the influence of physical processes on plume development (Textor et al., 2006). For a given volcanic forcing at the lower boundary ATHAM

predicts the evolution of the gas particle mixture within the atmosphere. The concept of active tracers means that particles such as ash and hydrometeors can occur in any concentration and directly influence the dynamics and thermodynamics of the system through the equation of state. By assuming an instantaneous exchange of momentum and heat the evolution of individual active tracers is coupled to the evolution of the momentum and temperature of the gas particle mixture strongly reducing the number of independent prognostic variables in the model. In this study, 2D simulations of volcanic plumes are performed using eight incompressible tracers. Hydrometeors are split into small cloud and larger precipitation particles, including both liquid and solid phases representing cloud water, cloud ice, rain and graupel. Two classes of gases, water vapor and sulfur dioxide, are simulated. Two tracers represent the size spectrum of tephra particles, ash particles and lapilli with volume mean diameters of 1.5 mm and 5 mm, respectively.

The description of cloud microphysical processes within ATHAM is based on a bulk concept so that the hydrometeor mass is predicted whereas number concentrations are determined from prescribed (cloud water and cloud ice) or diagnosed (rain and graupel) particle sizes.

In the present simulation the formation of aggregates through ash hydrometeor interaction is ignored. Instead, ash particles and hydrometeors are assumed to coexist within the same volume as independent particles. Terminal fall velocities of particles are calculated from prescribed or diagnosed effective radii representative for the volume mean radius of the assumed Gamma particle size distribution. Non-sphericity effects are considered by modifications of the drag coefficient (Textor et al., 2006).

It is worth pointing out that ATHAM is not a dispersal model. Dispersal models, such as PUFF, REMOTE, FLEXPART and FALL3D (e.g., Barsotti et al., 2008; Stohl et al., 1998), are widely used to forecast the dispersion of ash particles and gases based on prescribed meteorological conditions. Their use helps to track regions that are likely to be subjected to ash cloud. Dispersal models provide outputs on a large spatial scale (thousands of kilometers) typically every three or six hours. They are operatively used. ATHAM, in contrast, simulates the plume dynamics in the proximity of the vent (up to approximately one hundred kilometers away from the vent) with a temporal and spatial resolution in the order of seconds to minutes and several tens to hundred meters, respectively. These characteristics are particularly useful when an accurate description of the plume dynamics and microphysics is needed. Here ATHAM is utilized to provide a synthetic plume used to study the response of a microwave passive sensor.

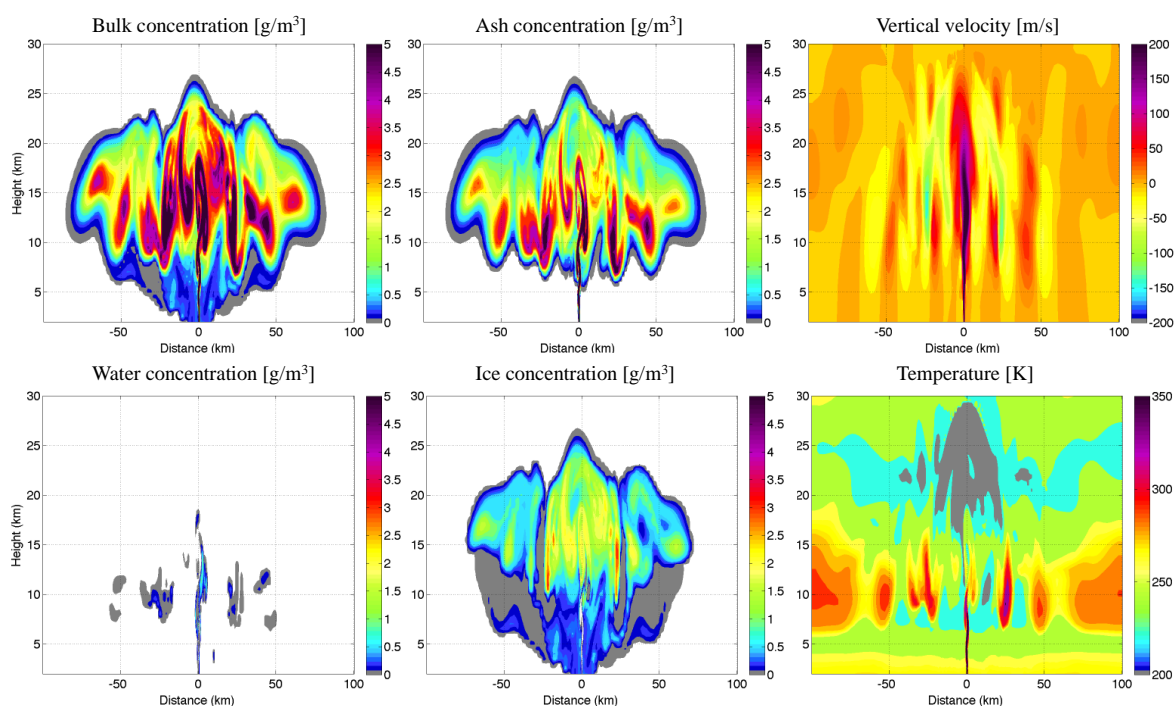


Fig. 1. Example of a volcanic plume simulation, in terms of mass concentrations (C_p), temperature and vertical wind, tuned for the 2011 Grímsvötn eruption event and obtained from ATHAM (Active Tracer High-Resolution Atmospheric Model) in

a bi-dimensional configuration (distance-altitude). Simulations refer to the volcanic plume after 26 min from the beginning of the eruption.

Figure 1 shows output from the 2D (altitude-distance) ATHAM simulation of the Grímsvötn eruption taken as reference scenario. ATHAM input parameters for this simulation are listed in **Table I**. The parameter selection has been done by comparing the ATHAM volcanic plumes with temporal sequences of radar vertical cross-sections from the 2011 Grímsvötn event. For this comparison, the ATHAM output has been first converted to radar reflectivity in the geometry of the actual radar measurements (i.e. in the polar coordinates). Thus, the ATHAM parameter selection has been accomplished by minimizing the bias between actual observed radar reflectivities and the ATHAM-derived reflectivities. Radar vertical cuts from one hour are used for the comparison between actual radar observations and ATHAM simulations. It should be mentioned that the validity of the comparison is limited to the radar sensitivity of coarse and larger particles (Marzano et al., 2010). However in the proximity of the volcanic vent (i.e., within approximately 50 km), larger particles are likely to dominate the radar backscattering signal. The nearest radiosonde site in Keflavík (station identifier: 04018 BIKF) at 00 Z, of May 21st, 2011, is used to initialize the ATHAM model. The microphysical particle characterization has been accomplished by using particle size distributions from past eruptions. For the analyzed simulations no crosswind effects (the initial horizontal wind component is set to zero) are taken into account while the terrain height is modeled through a Gaussian profile with standard deviation (std) and peak values specified as in **Table I**. Even though cross wind effects can significantly affect plume structure and microwave *BTs*, we tried to keep the simulations as simple as possible.

TABLE I. Input parameters for the ATHAM simulation

| Variable name | units | value |
|---------------------------------------|--------|-------|
| Height of the Gaussian vent | km] | .4 |
| Width (std) of the Gaussian vent | km] | 0 |
| Height of the Gaussian valley | km] | .08 |
| Width (std) of the Gaussian valley | km] | 0 |
| Initial velocity at the vent | m/s] | 00 |
| Potential temperature at the vent | K] | 13 |
| Specific water vapor concentration | kg/kg] | .090 |
| Specific sulfur dioxide concentration | kg/kg] | .010 |
| Specific cloud water concentration | kg/kg] | |
| Specific rain concentration | kg/kg] | |
| Specific cloud ice concentration | kg/kg] | |
| Specific graupel concentration | kg/kg] | |
| Specific small lapilli concentration | kg/kg] | .030 |
| Specific large lapilli concentration | kg/kg] | .070 |

Since output of ATHAM is provided on a stretched grid (i.e. fine grid spacing near the volcano vent and successively coarser resolution when moving away from the volcano vent to the lateral boundaries of the model domain), we performed a resampling of ATHAM output to obtain output on an evenly spaced grid. This is needed to be able to use ATHAM output as input for SDSU radiative

transfer simulator. The final vertical and horizontal grid spacing of the interpolated 2D outputs of ATHAM are 0.5 and 0.1 km, respectively.

2.1 Microwave sensor response simulator

Microwave passive simulations of volcanic plumes are obtained by using SDSU (Masunaga et al., 2010). SDSU is adopted as a forward model tool in the processes of constructing and testing performances of satellite algorithms for meteorological applications. SDSU is based on the delta-Eddington radiative transfer approximation, including both single and multiple scattering phenomena (Masunaga and Kummerow, 2005; Marzano, 2006). Mie routines for volume-equivalent spherical particles are used to compute the single-scattering optical parameters (extinction, albedo, and asymmetry factor), whereas simulated polarized radiances are derived using the delta-Eddington solution with polarization-dependent surface conditions. The space-based radiances (or antenna equivalent temperatures) are derived by convolving the antenna beam pattern with the simulated plume for a given spaceborne sensor specification. Note that SDSU is a pseudo-3D simulator since radiances are derived from single vertical columns projected along the observation nadir angle (i.e. slant path approximation). SDSU is capable to simulate not only satellite microwave passive sensors, but also infrared radiometers and microwave radar. It should be noted that fully 3D simulations, instead of pseudo-3D, would be ideal to investigate the impact of the slant path approximation. However, a rigorous treatment would require a significant increase in numerical complexity, requiring the coupling of a 3D ATHAM volcanic plume simulations with a fully 3D radiative transfer model which is beyond the scope of this report.

For volcanic applications, the input parameters of SDSU are adapted to work with the ATHAM numerical outputs. For convenience the adapted SDSU version is named SDSU-Ash. In its default configuration SDSU includes 6 microphysical species: graupel, hail, rain, cloud water, snow and cloud ice. They are described in terms of vertical profiles of concentrations C_p [g/m^3] of the respective microphysical species “ p ”, complex refractive index (n_p) as a function of wave length (λ), $n_p(\lambda) = n_p'(\lambda) - jn_p''(\lambda)$ and particle size distributions (PSDs) $N_p(D)$ of spherical particles of equivalent-diameter D . To adapt SDSU to treat volcanic plumes, two hydrometeors that are unlikely to occur in volcanic plumes are modified to mimic small ash and large lapilli. The values of C_p profiles, with $p=\text{snow}$ and $p=\text{hail}$ in SDSU, have been substituted with profiles of ash from ATHAM: $p=\text{SL}$ and $p=\text{LL}$ for Small Lapilli and Large Lapilli, respectively. $n_{SL}(\lambda)$ and $n_{LL}(\lambda)$ are adapted accordingly. The values of $n_{SL}(\lambda) = n_{LL}(\lambda) = n_{ash}(\lambda)$ are listed in **Table II** (Adams et al., 1996; Rogers et al., 2011).

TABLE II. Refractive Indexes Of Ash
(n_{ASH}' , n_{ASH}''): real and imaginary part of refractive index of ash, respectively.)

| Freq. | [20,190] GHz |
|-------------|--------------|
| n_{ASH}' | 2.48 |
| n_{ASH}'' | 0.016 |

For other species, namely graupel, rain, cloud water and cloud ice, a direct correspondence between ATHAM outputs and SDSU-Ash inputs has been assumed. Ash particle size distributions $N_p(D)$ are assumed to follow a Gamma distribution:

$$N_p(D) = N_{np} \left(\frac{6 \cdot (3.67 + \mu)^{\mu+4}}{3.67^4 \Gamma(\mu + 4)} \right) \left(\frac{D}{D_{np}} \right)^\mu \exp \left[- (3.67 + \mu) \left(\frac{D}{D_{np}} \right) \right] \quad (1)$$

where N_{np} , D_{np} and μ are the intercept parameter, volume-weighted median diameter and the shape parameter, respectively, in units of [m^{-4}], [mm] and [adim]. As a result, in SDSU-Ash the PSD $N_p(D)$ is given in [m^{-4}]. While D_{np} and μ are fixed, N_{np} is calculated from the knowledge of concentrations C_p and density (ρ_p) in [kg/m^3] through (Marzano et al., 2010):

$$N_{np} = \frac{C_p 10^{-3}}{\pi \rho_p} \left(\frac{3.67}{D_{np} 10^{-3}} \right)^4 \quad (2)$$

To be consistent with the ATHAM output, small lapilli (SL) and large lapilli (LL) PSDs have been assumed in SDSU-Ash for describing the ash classes. Their parameters are listed in **Table III** together with two additional ash classes namely:

TABLE III. PSD Parameters For ASH classes
 (D_{np} , μ , ρ_p : median diameter, shape parameter and concentration of Particle type “p” .)

| PSD param.: | D_{np} [mm] | μ [-] | ρ_p [kg m ⁻³] |
|----------------------|------------------|--------------|-----------------------------------|
| Fine Ash | 0.02 | 0.5 | 2.5×10^{-3} |
| Coarse Ash | 0.3 | 1.1 | 2.0×10^{-3} |
| Small Lapilli | 1.5 | 1.6 | 1.2×10^{-3} |
| Large Lapilli | 5.0 | 2.0 | 1.0×10^{-3} |

Fine Ash (FA) and Coarse Ash (CA), which are shown in **Figure 2** completeness and to match the observed PSD. In this figure the overall agreement of $N_p(D)$ in (1) and PSD parameters from Table III with in-situ PSD retrievals, relative to the 2004 Grímsvötn eruption, is shown for the case of $C_p=1 \text{ g/m}^3$. The measured PSD is derived from ash deposits collected close to the volcano vent (up to 60) and within a few years after the eruption. Consequently fine ash fraction of the erupted tephra may be underestimated. However, this doesn't affect simulated radar reflectivities since fine ash barely affects microwave radiation. Two additional assumptions are made when using PSDs ground measurements of tephra. The first assumption is that the PSD measured at the ground is representative of the PSD at the vent. The second assumption is that the sampling of PSD done after the eruption is still representative of what happened during the eruption itself. The last assumption is generally met in Iceland due to the snow cover preserving the deposited tephra.

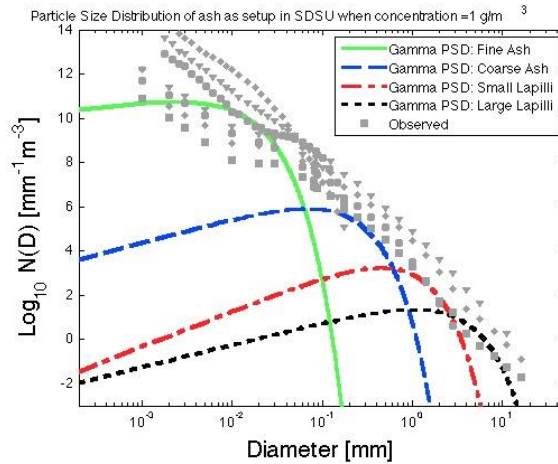


Fig. 2. Particle size distributions (PSDs) for volcanic ash. Grey markers refer to surface data, collected after the Grímsvötn volcanic eruption in 2004. PSDs Gamma model curves, given in (1) in the main text, are indicated by dotted and continuous lines with parameters listed in Table 3. The units of $N_p(D)$ are in $[\text{mm}^{-1} \text{m}^{-3}]$ since it is a more conventional choice for radar studies.

3. NUMERICAL RESULTS OF MICROWAVE SIMULATOR

In this section results are discussed in terms of microwave observations and their correlation with SDSU-Ash numerical simulations. Observations include microwave ground weather C-band radar estimates and SSMIS satellite passive measurements for the 2011 Grímsvötn eruption. The simulation results are produced from the coupled ATHAM plus SDSU-Ash forward model simulator with the aim to demonstrate the consistency between simulation and observational data. ATHAM coupled with

SDSU-ash is used to correlate brightness temperatures from satellite microwave radiometer and columnar ash concentrations of the scene. Thus, our goal is not to reproduce the space-time evolution of volcanic plume with the ATHAM model, but to provide a simulation that, when coupled with a radiative transfer model, can provide statistically consistent data for the interpretation of available radiometer observations.

3.1 Microwave brightness temperature simulations

In this section the analysis of the space-based microwave radiometric signatures of a volcanic plume is shown in terms of its consistency with the coupled forward model SDSU-Ash mentioned above. The considered radiometric instrument for the numerical simulations is the SSMIS. This leads to a straightforward comparison with the observations previously discussed. Our goal here is not to reproduce the observed signature of the SSMI scene using SDSU-Ash (as it would require specific knowledge of several geophysical and atmospheric parameters), but a self-consistency analysis i.e. the correlation and dynamic range of the SSMI BT_H channels.

Simulations of BT_H from the synthetic scenario, shown in Figure 1, have been generated using SDSU-Ash. The assumed refractive index for ash are listed in Table II. The PSDs are fixed to those that correspond to small and large lapilli (Table III) since they provided the best result in reproducing the observed correlation signatures (as it will be shown later). Additionally, it seems plausible to have larger grain size as a lapilli-type PSD near the volcanic source of an event as big as the 2011 Grímsvötn eruption. **Figure 3** shows the microwave brightness temperature at horizontal polarization over land (BT_{Hnd}) when the radiometer’s field of view intercepts the volcanic plume. Properties of the corresponding plume are shown in Figure 1. Terrain emissivity, fixed here to 0.7, is difficult to estimate. It depends on the type of surface vegetation and coverage (e.g. snow, sand etc.). In the microwave regime a terrain average emissivity of 0.9 is usually assumed in the absence of snow. During the 2011 Grímsvötn eruption snow was present on the ground which implies lower values for the terrain emissivity. As discussed below sensitivity tests confirm that a terrain emissivity of 0.7 is a reasonable choice in our case. In Figure 3 a depression in BT_{Hnd} can be noted near the volcanic vent. This phenomenon has been already observed before (Delene et al., 1996) and can be explained by the simultaneous presence of high ash and ice concentrations near the vent causing enhanced extinction of upwelling radiation from the ground.

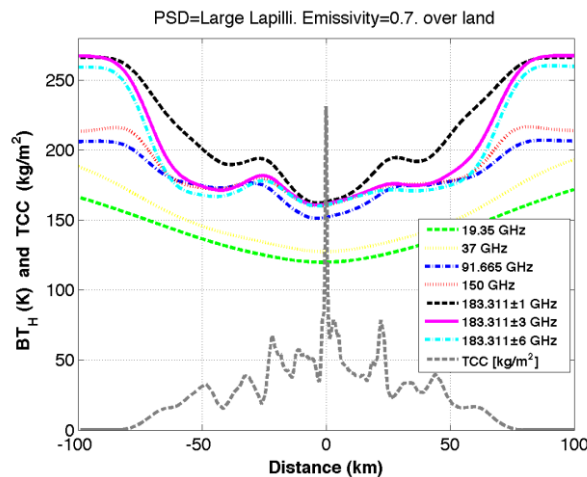


Fig. 3. Simulated brightness temperatures in horizontal polarization over land (BT_{Hnd}), for frequency channels as specified in the legend, vs. the distance from the volcano vent for the reference 2D-ATHAM (Active Tracer High-Resolution Atmospheric Model) synthetic plume shown in Fig. 1. BT_{Hnd} calculations have been done using the SDSU-Ash (Satellite Data Sensor Unit simulator for ash). Grey curve shows the ATHAM synthetic Total Columnar Content (TCC) in $[kg/m^2]$.

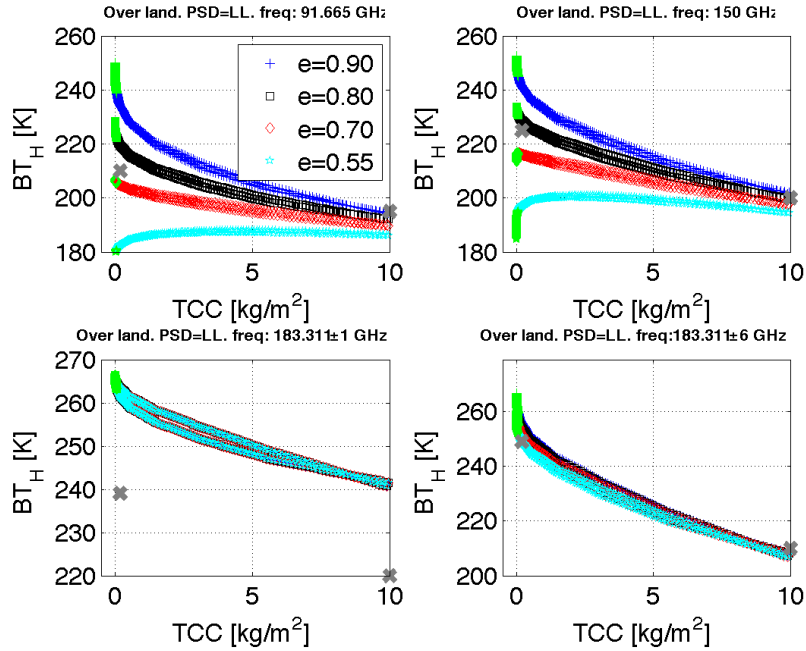


Fig. 4. Simulated brightness temperatures at horizontal polarization over land (BT_{Hnd}), for frequency channels as specified in the title of each panel and terrain emissivity (e) as listed in the legend, vs. the synthetic Total Columnar Content (TCC) in $[kg/m^2]$ from the 2D-ATHAM (Active Tracer High-Resolution Atmospheric Model) and SDSU-Ash (Satellite Data Sensor Unit simulator for ash) simulation. Grey crosses refer to the extremes of the linear regressions, as derived from the SSMIS (Special Sensor Microwave Imager/Sounder) and radar observations. The symbolism $f \pm x$ GHz, where f is the central frequency, refers to the received radiation in the interval $f-x$ and $f+x$ GHz. Green colored points on the left side in each panel refers to areas of the ATHAM simulation far from the volcanic plume shown in Figure 1.

Sensitivity tests with respect to PSD parameters listed in table III and terrain emissivity were also performed by determining the maximum values of BT_{Hnd} and the difference between maximum and the minimum values of BT_{Hnd} , named MBT_{Hnd} and DBT_{Hnd} , respectively. Values for MBT_{Hnd} are found to decrease or remain constant as the PSD varies from FA to LL with lower frequencies being more sensitive to PSD parameters than higher frequencies. The variations of MBT_{Hnd} can be as large as 30 K at 19 GHz and less than 1 K at 183 ± 6 GHz. The difference quantity DBT_{Hnd} is a measure of the scattering and extinction effects induced by the volcanic cloud. As evident, DBT_{Hnd} increases as particle size increases for frequencies below 37 GHz with differences up to 60 K. For frequencies greater than 37 GHz no clear trend of DBT_{Hnd} as a function of particle size is observed, since Mie scattering becomes size independent at higher frequencies. In this case, variations in DBT_{Hnd} of up to 45 K are found.

3.2 Ash loading estimate and surface emission sensitivity

Considering the larger dynamic range of BT_{Hnd} for channels above 90 GHz, together with their better spatial resolution than those below 90 GHz, correlation between the simulated BT_{Hnd} at 91.6 GHz, 150.0 GHz, 183 ± 1 GHz, and 183 ± 6 GHz and the TCC of the simulated volcanic plume are calculated. Trends of BT_{Hnd} with TCC are shown in **Figure 4** for values of terrain emissivity (e) between 0.55 and 0.90. The effects of the terrain emissivity are relevant at 91 GHz and 150 GHz, whereas they are less influential for frequencies close to the water vapor absorption peak (i.e., 183 GHz) as becomes evident by the small variations of BT_{Hnd} as a function of e at those frequencies. In Figure 4 the values of BT_{Hnd} where TCC approaches 0, refer to the areas of the ATHAM simulation far away from the volcanic plume. In these areas the absorption of water vapor drives the BT_{Hnd} response. Excluding these areas from the analysis (marked as green), **Table IV** lists the linear regression coefficients of BT_{Hnd} as a function of TCC .

TABLE IV. BT_H vs T_{CC} Regression Parameters from simulations

$$BT_{H_{\text{land}}} = a \cdot (TCC) + b, \quad TCC \text{ [kg/m}^2\text{]}; \quad BT_{H_{\text{land}}} \text{ [K]}$$

| Freq. [GHz] | $e=0.55$ | $e=0.70$ | $e=0.8$ | $e=0.9$ |
|--------------|------------|------------|------------|------------|
| | a / b | a / b | a / b | a / b |
| 91 | 0.3 / 186 | -1.7 / 205 | -3.0 / 218 | 4.4 / 231 |
| 150 | -0.4 / 201 | -2.1 / 218 | -3.2 / 229 | -4.3 / 239 |
| 183±1 | -2.3 / 261 | -2.3 / 261 | -2.3 / 261 | -2.3 / 261 |
| 183±6 | -4.7 / 249 | -4.9 / 251 | -5.0 / 252 | -5.7 / 253 |

($BT_{H_{\text{land}}}$: Brightness temperature in horizontal polarization over land; TCC : Total Columnar Content.)

3.3 Considerations

The Active Tracer High-Resolution Atmospheric Model (ATHAM) and the Satellite Data Simulation Unit (SDSU) radiative transfer model is coupled after some adjustments to ingest volcanic plumes (instead of water clouds) into SDSU. The main conclusions are that i) the ATHAM /SDSU-ash models provides results that are consistent with the SSMIS observations in all wavelengths except for 183±1 GHz where the 2D version of ATHAM produces temperature and humidity profiles that are inconsistent with observed radiosonde profiles; ii) the model-driven estimator of plume height provides results consistent with observations even though its accuracy is subject to model uncertainty. These results support the conclusion that it is in principle possible to estimate the total columnar content of an ash cloud near the volcano source vent from a multi-frequency measurement of the satellite brightness temperature over land at horizontal polarization.

The capability to estimate plume height near the volcanic vent based on measured brightness temperatures can improve estimates derived from the ground radar. Volcanic plumes are composed of several scatterers, not just ash, with different properties. The combination of multi-frequency satellite and ground-based retrievals can help to better sample ash particle spectra. In this context, satellite infrared retrievals of plume height can also be used to infer size information due to their sensitivity to very fine ash particles since plume height estimates are frequency-dependent. Ground based radars in contrast are not sensitive to the smallest ash particles.

4. IMPROVED INFRARED RETRIEVAL OF ASH MASS LOADING

The reverse absorption technique is often used to detect volcanic ash clouds from thermal infrared satellite measurements. The difference between brightness temperatures (ΔT) at 10.8 ($T_{10.8}$) and 12 μm (T_{12}) for volcanic ash clouds is negative in contrast to liquid-water and ice clouds, which give positive brightness temperature differences. Assuming spherical ash particles composed of andesite and a monodisperse size distribution, Wen and Rose(1994) showed that the particle radius has to be below 5 μm to give a negative ΔT . This implies that for andesite the particles in a given size distribution (for example log-normal) that contribute to the negative ΔT , have radii $<5 \mu\text{m}$. The effective radius, defined as the ratio of the third and second moment of the size distribution, may be larger than 5 μm depending on the form of the distribution. Effective radii $>5 \mu\text{m}$ estimated from infrared (IR) satellite measurements have been reported by several authors (see for example Yu et al., 2002; Corradini et al., 2008; Francis et al., 2012; Pavolonis et al, 2013). For retrieval of ash mass loading and effective radius, it is common to assume that the ash particles are spherical and thus use Mie theory to calculate the optical properties (e.g. extinction cross section, single scattering albedo and asymmetry factor, Prata, 1989; Wen and Rose, 1994; Clarisse et al., 2010b; Prata and Prata, 2012; Pavolonis et al, 2013). It is well established that, over a large range of radii, wavelengths, and dielectric properties, the optical properties of non-spherical particles can be significantly different from those of spherical particles (for a readable and general introduction into the vast field of scattering by non-spherical particles see the recent review by Mishchenko, 2009). The non-sphericity of particles residing in the Earth's atmosphere may affect the signal measured by satellites and as such have an impact on the quantity, which is being remotely sensed, e.g. the mass of a volcanic ash cloud.

Krotkov et al. (1999) used randomly oriented spheroids to test the sensitivity of Total Ozone Mapping Spectrometer (TOMS) retrieval of ash cloud optical depth and effective radius. The TOMS observes backscattered solar radiation in the 0.34-0.38 μm spectral interval. The assumption of spherical particles underestimates the effective radius by up to 30% and overestimates the optical depth by up to 25%. The total mass of the ash cloud is underestimated by 5-20%. The UV volcanic ash refractive index used in that study, $m=1.5-0.005i$, is different from that found in the thermal infrared where both the real and imaginary parts of the refractive index are higher, (e.g. $m=2.11-0.59i$ at 10.8 μm and $m=1.83-0.13i$ at 12 μm for andesite according to Pollack et al.,1973). If the material of the particles is optically hard (large real part) or strongly absorbing (large imaginary part), particularly the roughness of the particle, not considered by Krotkov et al. (1999), may play an important role for the optical properties (e.g. Kahnert et al., 2011; Kahnert et al., 2012). Also, TOMS measures solar radiation backscattered by the atmosphere and its constituents, while IR detectors, such as the Spinning Enhanced Visible and Infrared Imager (SEVIRI), the Moderate Resolution Imaging Spectroradiometer (MODIS), the Advanced Very High Resolution Radiometer (AVHRR), and the Infrared Atmospheric Sounding Interferometer (IASI) measure the radiation emitted by the Earth's surface and atmosphere. Thus, the results in the UV may not be directly transferable to the thermal infrared.

In the IR the influence of particle shape has been investigated for mineral dust aerosol and polar stratospheric clouds. Hudson et al., (2008a) and Hudson et al., (2008b) found that for particles in the fine particle mode, radius 0.05-2 μm , ellipsoid particles and disk-shaped models better reproduced experimental mineral component IR spectra compared to Mie theory calculations for non-clay and clay components of mineral dust aerosol, respectively. Kluser et al. (2012) used these measured mineral component IR spectra, which include non-spherical effects and also variable mineral composition, in Infrared Atmospheric Sounder Interferometer (IASI) retrievals of desert dust aerosol optical depth, and found significant improvements in agreement with Aerosol Robotic Network (AERONET) observations. Similar shape effects in the infrared have earlier been shown for polar stratospheric clouds by Wagner et al. (2005).

To our knowledge only Newman et al. (2012) have investigated the effects of non-sphericity of volcanic ash particles in the infrared. They compared optical properties of equal volume spheres with those of randomly oriented hexagonal columns of aspect ratio unity as calculated by the T-matrix method. Differences between the optical properties of the spheres and the hexagonal columns were reported to be less than 10% which was considered not significant for their purposes (lidar-derived

aerosol extinction and ash mass concentration to be used in a radiative closure study). It is noted that Yang et al. (2007) have compared radiative properties of dust-like spheroids and spheres at thermal infrared wavelengths and concluded that the effect of non-sphericity was not significant. They based their conclusion on comparisons of brightness temperatures from simulations with spheres and spheroids and did not estimate the error on retrieved quantities.

Scanning-electron-microscope images of volcanic ash particles show the highly irregular shapes of the particles (see for example Riley et al., 2003; Muñoz et al., 2004; Schumann et al., 2011; Weber et al., 2012; Genareau et al. 2013). The shapes may be divided into three wide categories: vesicular, non-vesicular and miscellaneous shapes (Riley et al., 2003). Vesicular shapes may be present up to hundreds of km from the volcano (Muñoz et al., 2004). For the Eyjafjallajökull 2010 eruption, vesicular shapes were present close to the volcano (about 50 km), while non-vesicular shapes appeared to be dominant thousands of kilometers away from the vent (Schumann et al., 2011; Weber et al., 2012). Here it is investigated how highly irregular and porous (vesicular) ash particles affect the thermal radiation measured by satellites and the impact on derived quantities such as ash mass loading. This is achieved by performing thermal infrared radiative transfer calculations with non-spherical ash particles and comparing with calculations using mass and volume equivalent spherical particles.

5. ASH PARTICLE OPTICAL PROPERTIES

To calculate the ash particle optical properties, model geometries for the ash particles are first generated. These geometries are then used in the single-scattering computations.

5.1 Particle shapes

Two distinct ash particle geometries are considered: vesicular ash particle shapes from Lindqvist et al. (2011) and porous spheroids from Nousiainen et al. (2011). The former model results in irregularly shaped particles, while in the latter the overall shape of the particles is spheroidal. Both types of particles are porous, that is, the generated model particles have hollow internal cavities.

In case of vesicular ash particles, particles with both small and large vesicles (porous cavities) are considered. The parameter values for generation of these phenomenological model particles (Kylling et al. 2014) have been selected based on visually inspecting scanning-electron microscope images of real volcanic ash particles (Riley et al., 2003; Muñoz et al., 2004). Porous spheroids have the shape of normal spheroids, but they are filled with spherical vesicles.

The porosity p of a particle describes the fractional volume of the cavities within the particle. For the large-vesicle ash shapes, porosity varies between $p=0.41-0.60$ and, for small-vesicle ash, $p=0.29-0.31$. Both spheroids with small cavities have porosity $p=0.44$ while the porosity of large-cavity spheroids is $p=0.48-0.50$. For further details of the model particle generation, see the original publications by Lindqvist et al. (2011) and Nousiainen et al. (2011).

5.2 Single scattering optical properties

The optical properties of the non-spherical ash particles were calculated by the discrete dipole approximation (DDA), using the DDSCAT program (Draine and Flatau, 1994 and 2012). The discrete dipole method is a volume-integral equation method, in which the volume integral is numerically evaluated by discretizing the particle volume into (usually cubical) volume cells with side length d . The main assumption is that d is sufficiently small, so that the electric field can be assumed to be constant over each cell volume. Thus, the oscillators within each volume cell respond to the external field by oscillating in phase, just like a dipole, and phase differences may arise only between cells. This means that in the DDA the target is, essentially, replaced by an array of dipoles with a dipole spacing d . Calculations of the optical properties for the 14 geometries were made for 10 mass

equivalent radii of 1, 2, ..., 10 μm , and for 2 IR wavelengths, 10.8 and 12 μm . The refractive index for andesite from Pollack et al. (1973) was used.

For comparison, computations for mass- and volume-equivalent spheres were performed with a standard Mie program (Mishchenko et al., 2002). To compare these against the results based on non-spherical ash particles, the following two types of size equivalences were considered:

1. Mass-equivalent spheres with the same refractive index as andesite.
2. Volume-equivalent spheres with average andesite volume fractions of 50 % for particles with large vesicles and 70 % for particles with small vesicles. The vesicles were assumed to be gas pockets with a refractive index of $m=1$. In each case an effective refractive index was calculated using the Maxwell Garnett mixing rule (Maxwell, 1904) or the Bruggeman mixing rule (Bruggeman 1935).

6. INFRARED RADIATIVE TRANSFER SIMULATION SETUP AND RESULTS

To calculate the brightness temperature for satellite geometry the libradtran package was utilized (www.libradtran.org and Mayer and Kylling, 2005). The ash cloud was vertically homogeneous, 1 km thick, and with the cloud top at 10 km. The sub-arctic summer atmosphere (Anderson et al., 1986) was adopted as the ambient atmosphere, thus giving a temperature of 225 K at 10 km and a surface temperature of 280 K. The emissivity of the surface was set to 0.98, which is representative for water at the wavelengths considered. Gaseous absorption was not included. Accurate treatment of the ash particle phase functions were assured by using the improved discrete-ordinate (DISORT) method by Buras et al (2011), which is based on the versatile and much used DISORT algorithm by Stamnes et al (1988). The improved DISORT code was run with 16 streams. A mono-disperse particle size distribution was used. Brightness temperatures were calculated for wavelengths 10.8 and 12.0 μm representative for the central wavelengths for channels 9 and 10 of SEVIRI, for various ash optical depths and mass-equivalent particle radii.

6.1 Numerical results

In Fig. 5, $T_{10.8}$ is shown versus the brightness temperature difference for a few representative particle shapes for nadir view. The solid lines in Fig. 5 represent various mass-equivalent particle radii whose values are indicated in black. The dotted blue lines indicate various ash optical depths whose values are given in blue.

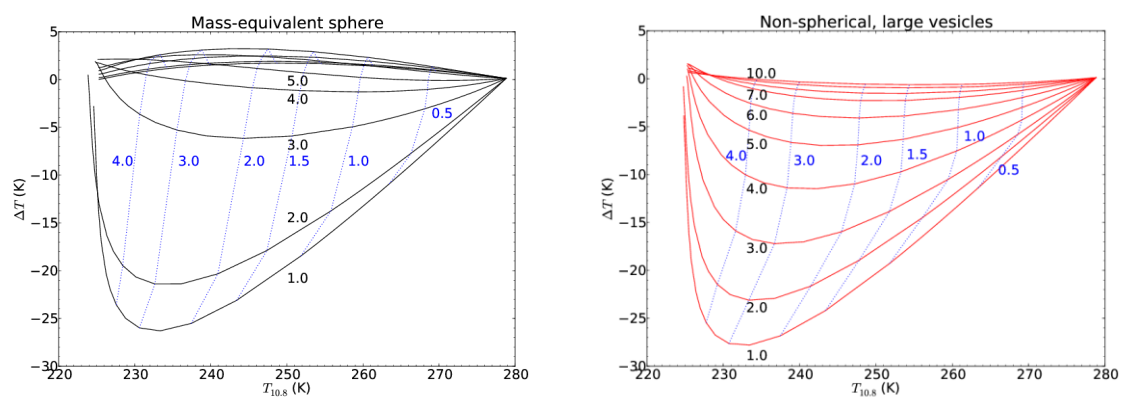


Fig 5. The brightness temperature ($T_{10.8}$) at 10.8 μm versus the brightness temperature difference (ΔT) for various model ash particle types. Black colored numbers label mass-equivalent particle radius (μm) isolines (black). Blue numbers are ash cloud optical depth (dotted blue lines).}

The left plot is similar to those used to visualize the retrieval of ash mass loading and effective radius from $T_{10.8}$ and T_{12} measurements under the assumption of spherical ash particles (Wen and

Rose, 1994; Prata and Prata, 2012). The right plot in Fig. 5 shows ΔT versus $T_{10.8}$ for non-spherical ash particles with large vesicle. The results for the other non-spherical shapes are similar.

6.2 Discussion

Information about volcanic ash in the atmosphere from infrared measurements may be deduced in a two-step process. First ash affected pixels are detected, secondly the ash physical properties are retrieved from ash affected pixels.

The detection of ash by the reverse absorption technique is based on the different spectral behaviour of the extinction coefficients of volcanic ash, liquid-water and ice clouds and the trace gases in the atmosphere (Prata, 1989). A negative ΔT indicates volcanic ash whereas liquid-water and ice clouds give positive ΔT . The non-spherical ash particles in this study give negative ΔT for a wider range of particle sizes than mass-equivalent spherical particles. Thus, assuming that the non-spherical particles are a better representation of the real world compared to mass-equivalent spherical particles, nature produces negative ΔT for a larger size range than modelled spherical particles.

The mass loading of a pixel may be calculated from the effective radius and the ash cloud optical depth (Wen and Rose, 1994). For a given combination of ΔT and $T_{10.8}$ the optical depth and effective radius may be found from charts similar to those shown in Fig. 1. Usually mass-equivalent spheres, left plot, are used for retrieval of ash optical properties. The use of any of the other ash particle shapes will give a different ash mass loading.

In the left plot of Fig. 6 is shown the ash mass loading retrieved from SEVIRI 10.8 and 12.0 μm channel measurements for a case during the Eyjafjallajökull 2010 eruption. The retrieval was made using an optimal estimation technique and non-spherical ash particles with large vesicles were assumed. Furthermore, a mono-disperse size distribution was used. For comparison retrievals were also made assuming mass-equivalent spheres. The difference between the ash mass loading when using the two types of model particles is shown in the right plot of Fig. 2. For all pixels the non-spherical particles give a larger ash mass loading compared to the mass-equivalent spheres.

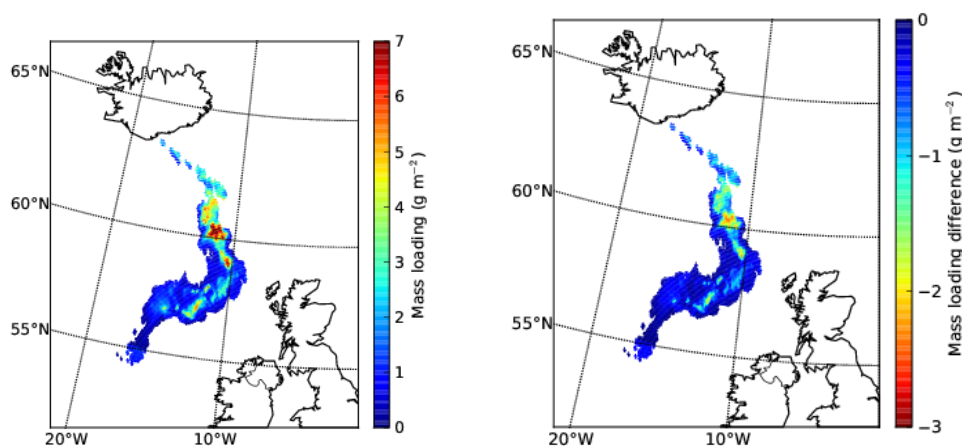


Fig. 6. (Left) The ash mass loading for 1900 UTC on 6th May 2010 during the Eyjafjallajökull eruption. The ash mass loading was derived assuming non-spherical ash particles with large vesicles. (Right) The difference ($=(\text{spherical mass-equivalent spheres}) - (\text{non-spherical ash particles})$) in ash mass loading between retrievals using mass-equivalent spheres and non-spherical ash particles with large vesicles.

The uncertainty in the total mass of the ash cloud due to the assumption of particle shape and the treatment of porosity may be compared with the uncertainties in total mass arising from the lack of knowledge in other contributing factors (surface temperature, surface emissivity, plume geometry and altitude, aerosol type, atmospheric water vapor). Corradini et al. (2008) have estimated that typical uncertainty in total mass estimates due to these other factors are on the order of 40 %. The total mass for the case in Fig. 2 retrieved with non-spherical ash model particles (mass-equivalent spheres) is

3.47e+08 kg (2.48e+08 kg). Mass-equivalent spheres thus underestimate the total mass by about 30%. The particle shape is thus as important as the other, previously considered factors. Assuming independent uncertainties the total uncertainty in the total mass is given by the square root of the sum of the squared uncertainties. Adding the uncertainty due to shape to the other sources of uncertainty, the uncertainty of the total mass increases from 40% to about 50%.

REFERENCES

- Adams R. J., W. F. Perger, W. I. Rose, A. Kostinski, "Measurements of the complex dielectric constant of volcanic ash from 4 to 19 GHz", *Journal of Geophysical Research*, vol. 101, issue B4, pp. 8175-8185, 1996.
- Anderson, G., Clough, S., Kneizys, F., Chetwynd, J., and Shettle, E., "AFGL atmospheric constituent profiles (0-120 km)", *Tech. Rep. AFGL-TR-86-0110*, Air Force Geophys. Lab., Hanscom Air Force Base, Bedford, Mass., 1986.
- Barsotti S., A. Neri, J. S. Scire, "The VOL-CALPUFF model for atmospheric ash dispersal: 1. Approach and physical formulation", *Journal of Geophysical Research*, vol. 113, issue B3, pp. 1-12, 2008.
- Bruggeman, D. A. G., "Berechnung verschiedener physikalischer Konstanten von heterogenen Substanzen. 1. Dielektrizitätskonstanten und Leitfähigkeiten der Mischkörper aus isotropen Substanzen, *Ann. Phys.*, 24, 636-664, 1935.
- Buras, R., Dowling, T., and Emde, C., "New secondary-scattering correction in DISORT with increased efficiency for forward scattering, *J. Quant. Spectrosc. Radiat. Transfer*, 112, 2028-2034, doi: 10.1016/j.jqsrt.2011.03.019, 2011.
- Clarisse, L., Hurtmans, D., Prata, A. J., Karagulian, F., Clerbaux, C., Mazière, M.-D., and Coheur, P.-F., "Retrieving radius, concentration, optical depth, and mass of different types of aerosols from high-resolution infrared nadir spectra, *Appl. Opt.*, 49, 3713-3722, 2010.
- Corradini, S., Spinette, C., Carboni, E., Tirelli, C., Buongiorno, M. F., Pugnaghi, S., and Gangale, G., "Mt. Etna tropospheric ash retrieval and sensitivity analysis using Moderate Resolution Imaging Spectroradiometer Measurements, *J. of Applied Remote Sensing*, 2, doi:10.1117/1.3046, 674, 2008.
- Delene D. J., W. I. Rose, N. C. Grody, "Remote sensing of volcanic clouds using special sensor microwave imager data", *Journal of Geophysical Research*, vol. 101, issue B5, pp. 11579-11588, 1996.
- Draine, B. T. and Flatau, P. J., "Discrete dipole approximation for scattering calculations, *J. Opt. Soc. Am.*, 11, 1491-1499, 1994.
- Draine, B. T. and Flatau, P. J., "User Guide to the Discrete Dipole Approximation Code DDSCAT 7.2, <http://arXiv.org/abs/1202.3424>, 2012.
- Francis, P. N., Cooke, M. C., and Saunders, R. W., "Retrieval of physical properties of volcanic ash using Meteosat: A case study from the 2010 Eyjafjallajökull eruption", *J. Geophys. Res.*, 117, doi:10.1029/2011JD016788, 2012.
- Gangale G., A. J. Prata, L. Clarisse, "The infrared spectral signature of volcanic ash determined from high-spectral resolution satellite measurements", *Remote Sensing of Environment*, vol. 114, pp. 414-425, 2010.
- Genareau, K., Mulukutla, G., Proussevitch, A., Durant, A., Rose, W., and Sahagian, D., "The size range of bubbles that produce ash during explosive volcanic eruptions, *Journal of Applied Volcanology*, 2, 4, doi: 10.1186/2191-5040-2-4, 2013.
- Grody N.C., A. N. Basist, "Global identification of snow cover using SSM/I measurements", *IEEE Transactions on Geoscience and Remote Sensing*, vol. 34, issue 1, pp. 237-249, 1996.
- Hudson, P. K., Gibson, E. R., Young, M. A., Kleiber, P. D., and Grassian, V. H., "Coupled infrared extinction and size distribution measurements for several clay components of mineral dust aerosol, *Journal of Geophysical Research: Atmospheres*, 113, doi:10.1029/2007JD008791, 2008a.
- Hudson, P. K., Young, M. A., Kleiber, P. D., and Grassian, V. H., "Coupled infrared extinction spectra and size distribution measurements for several non-clay components of mineral dust aerosol (quartz, calcite, and dolomite), *Atmospheric Environment*, 42, 5991 - 5999, doi: /10.1016/j.atmosenv.2008.03.046, 2008b.
- Kahnert, M., Nousiainen, T., and Mauno, P., "On the impact of non-sphericity and small-scale surface roughness on the optical properties of hematite aerosols, *J. Quant. Spectrosc. Radiat. Transfer*, 112, 1815-1824, 2011.
- Kahnert, M., Nousiainen, T., Thomas, M. A., and Tyynelä, J., "Light scattering by particles with small-scale surface roughness: comparison of four classes of model geometries", *J. Quant. Spectrosc. Radiat. Transfer*, 113, 2356-2367, 2012.
- Klüser, L., Kleiber, P., Holzer-Popp, T., and Grassian, V., "Desert dust observation from space - Application of measured mineral component infrared extinction spectra, *Atmospheric Environment*, 46, 419 - 427, doi: /10.1016/j.atmosenv.2012.02.011, 2012.
- Krotkov, N., Flittner, D., Krueger, A., Kostinski, A., Riley, C., Rose, W., and Torres, O., "Effect of particle non-sphericity on satellite monitoring of drifting volcanic ash clouds, *J. Quant. Spectrosc. Radiat. Transfer*, 63, 613-630, doi:10.1016/S0022-4073(99)00041-2, 1999.
- Kylling, A., M. Kahnert, H. Lindqvist and T. Nousiainen, "Volcanic ash infrared signature: porous non-spherical ash particle shapes compared to homogeneous spherical ash particles", *Atmos. Meas. Tech.*, in press, 2014.

- Lindqvist, H., Nousiainen, T., Zubko, E., and Muñoz, O., "Optical modeling of vesicular volcanic ash particles", *Journal of Quantitative Spectroscopy and Radiative Transfer*, 112, 1871-1880, doi:10.1016/j.jqsrt.2011.01.032, 2011.
- Marzano F.S., "Modeling antenna noise temperature due to rain clouds at microwave and millimeter-wave frequencies", *IEEE Trans. Antennas and Propagat.*, vol. 54, pp. 1305-1317, 2006.
- Marzano F.S., S. Marchiotti, C. Textor and D. Schneider, "Model-based Weather Radar Remote Sensing of Explosive Volcanic Ash Eruption", *IEEE Trans. Geosci. Rem. Sensing*, vol. 48, pp. 3591-3607, 2010.
- Masunaga H., T. Matsui, W.-K. Tao, A. Y. Hou, C. D. Kummerow, T. Nakajima, P. Bauer, W. S. Olson, M. Sekiguchi, T. Y. Nakajima, "Satellite Data Simulator Unit a multisensor, multispectral satellite simulator package", *Bulletin of the American Meteorological Society*, vol. 91, issue 12, pp. 1625-1632, 2010.
- Masunaga H. and C. D. Kummerow, 2005: Combined radar and radiometer analysis of precipitation profiles for a parametric retrieval algorithm. *J. Atmos. Oceanic Technol.*, 22, 909-929.
- Maxwell Garnett, J. C., "Colours in metal glasses and in metallic films, *Philos. Trans. R. Soc. A*, 203, 385-420, 1904.
- Mayer, B. and Kylling, A., "Technical note: the libRadtran software package for radiative transfer calculations-description and examples of use, *Atmos. Chem. Phys.*, 5, 1855-1877, 2005.
- Mishchenko, M. I., "Electromagnetic scattering by nonspherical particles: A tutorial review, *J. Quant. Spectrosc. Radiat. Transfer*, 110, 808-832, 2009.
- Mishchenko, M. I., , Travis, L. D., and Lacis, A. A., "Scattering, absorption, and emission of light by small particles, Cambridge University Press, Cambridge, 2002.
- Muñoz, O., Vollen, H., Hovenier, J. ., Veihelmann, B., van der Zande, W. ., Waters, L. B. F. ., and Rose, W.I., "Sattering matrices of volcanic ash particles of Mount St. Helens, Redoubt, and Mount Spurr volcanoes, *J. Geophys. Res.*, 109, doi:0.1029/2004JD004684, 2004.
- Newman, S. M., Clarisse, L., Hurtmans, D., Marenco, F., Johnson, B., Turnbull, K., Havemann, S., Baran, A.-J., O'Sullivan, D., and Haywood, J., "A case study of observations of volcanic ash from the Eyjafjallajökull eruption: 2. Airborne and satellite radiative measurements, *J. Geophys. Res.*, 117, D00U13, doi:10.1029/2011JD016780, 2012.
- Nousiainen, T., Kahnert, M., and Lindqvist, H., "Can particle shape information be retrieved from light-scattering observations using spheroidal model particles?", *J. Quant. Spectrosc. Radiat. Transfer*, 112, 2213-2225, doi:10.1016/j.jqsrt.2011.05.008, 2011.
- Oberhuber J.M., M. Herzog, H.F. Graf, K. Schwanke, "Volcanic plume simulation on large scales", *Journal of Volcanology and Geothermal Research*, vol. 87, pp. 29-53, 1998.
- Pavolonis, M. J., Heidinger, A. K., and Sieglaff, J., "Automated retrievals of volcanic ash and dust cloud properties from upwelling infrared measurements", *J. Geophys. Res.*, 118, 1-23, doi:10.1002/jgrd.50173, 2013.
- Pollack, J. B., Toon, O. B., and Khare, B. N., "Optical properties of some terrestrial rocks and glasses, *ICARUS*, 19, 372-389, 1973.
- Prata, A. J. and Prata, A. T.: Eyjafjallajökull volcanic ash concentrations determined using Spin Enhanced Visible and Infrared Imager measurements, *J. Geophys. Res.*, 117, D00U23, doi:10.1029/2011JD016800, 2012.
- Prata, A.J., "Infrared radiative transfer calculations for volcanic ash clouds", *Geophys. Res. Lett.*, 16, 1293-1296, 1989.
- Riley, C. M., Rose, W. I., and Bluth, G. J. S., "Quantitative shape measurements of distal volcanic ash", *Journal of Geophysical Research: Solid Earth*, 108, doi:10.1029/2001JB000818, 2003.
- Rogers A. B., D. G. Macfarlane, D. A. Robertson, "Complex permittivity of volcanic rock and ash at millimeter wave frequencies", *IEEE Geoscience and Remote Sensing Letters*, vol. 8, issue 2, pp. 298-302, 2011.
- Schäuble, D., Tafferner, A., Rautenhaus, M., Gerz, T., Ziereis, H., Krautstrunk, M., Mallaun, C., Gayet, J.-F., Lieke, K., Kandler, K., Ebert, M., Weinbruch, S., Stohl, S., Gasteiger, K., Gross, S., Freudenthaler, V., Schumann, U., Weinzierl, B., Reitebuch, O., Schlager, H., Minikin, A., Forster, C., Baumann, R., Sailer, T., Graf, K., Mannstein, H., Voigt, C., Rahm, S., Simmet, R., Scheibe, M., lichtenstern, M., Stock, P., Rüba, H.,
- Stamnes, K., Tsay, S.-C., Wiscombe, W., and Jayaweera, K., "Numerically stable algorithm for discrete-ordinate-method radiative transfer in multiple scattering and emitting layered media, *Appl. Opt.*, 27, 2502-2509, 1988.
- Stohl A., M. Hittenberger, G. Wotawa, "Validation of the Lagrangian particle dispersion model FLEXPART against large scale tracer experiment data". *Atmospheric Environment.*, vol. 32, issue 24, pp. 4245-4264, 1998.
- Textor C., H. F. Graf, M. Herzog and J. M. Oberhuber, "Injection of gases into the stratosphere by explosive volcanic eruptions", *Journal of Geophysical Research*, vol. 108, N. D19, pp. 1-17, 2003.

- Textor C., H. F. Graf, M. Herzog, J. M. Oberhuber, W. I. Rose, G. G. J. Ernst, "Volcanic particle aggregation in explosive eruption columns. Part I: Parameterization of the microphysics of hydrometeors and ash", *Journal of Volcanology and Geothermal Research*, vol. 150, issue 4, pp.359-377, 2006.
- Wagner, R., Möhler, O., Saathoff, H., Stetzer, O., and Schurath, U.: "Infrared Spectrum of Nitric Acid Dihydrate: Influence of Particle Shape", *The Journal of Physical Chemistry A*, 109, 2572-2581, doi:10.1021/jp044997u, 2005.
- Weber, K., Eliasson, J., Vogel, A., Fischer, C., Pohl, T., van Haren, G., Meier, M., Grobety, B., and Dahmann, D., "Airborne in-situ investigations of the Eyjafjallajökull volcanic ash plume on Iceland and over north-western Germany with light aircrafts and optical particle counters", *Atmospheric Environment*, 48, 9-21, doi:10.1016/j.atmosenv.2011.10.030, , 2012.
- Wen S., W. I. Rose, "Retrieval of sizes and total masses of particles in volcanic clouds using AVHRR bands 4 and 5", *Journal of Geophysical Research*, vol. 99, issue D3, pp. 5421-5431, 1994.
- Wen, S. and Rose, W. I., "Retrieval of sizes and total masses of particles in volcanic clouds using AVHRR bands 4 and 5", *J. Geophys. Res.*, 99, 5421-5431, 1994.
- Wiegner, W., Ansmann, A., Tesche, M., Olafsson, H., and Sturm, K., "Airborne observations of the Eyjafjalla volcano ash cloud over Europe during air space closure in April and May 2010", *Atmos. Chem. Phys.*, 11,doi:10.5194/acp-11-2245-2011, 2011.
- Yang, P., Feng, Q., Hong, G., Kattawar, G. W., Wiscombe, W. J., Mishchenko, M. I., Dubovik, O., Laszlo, I., and Sokolik, I. N., "Modeling of the scattering and radiative properties of nonspherical dust-like aerosols", *J. Aerosol. Sci.*, 38, 995-1014, 2007.
- Yu, T., Rose, W. I., and Prata, A. J., "Atmospheric correction for satellite-based volcanic ash mapping and retrievals using "split window" IR data from GOES and AVHRR", *J. Geophys. Res.*, 107, doi:10.1029/2001JD000706, 2002.